Optofluidic ring resonator switch for optical particle transport†

Allen H. J. Yang[a] and David Erickson*[b]

Received 25th September 2009, Accepted 9th December 2009
First published as an Advance Article on the web 7th January 2010
DOI: 10.1039/b920006a

In this work, we demonstrate an optofluidic switch using a microring resonator architecture to direct particles trapped in the evanescent field of a solid-core waveguide. When excited at the resonant wavelength, light inserted into the bus waveguide becomes amplified within the ring structure. The resulting high optical intensities in the evanescent field of the ring generate a gradient force that diverts particles trapped on the bus to the ring portion of the device. We show that this increase in optical energy translates to an increase of 250% in the radiation pressure induced steady-state velocity of particles trapped on the ring. We also characterize the switching fraction of the device, showing that 80% of particles are diverted onto the ring when the device is at an on-resonance state. The optofluidic switch we present here demonstrates the versatility in exploiting planar optical devices for integrated particle manipulation applications.

Introduction

The fundamental principle behind the development of the lab-on-a-chip is to integrate numerous functions on a single device with the goal of reducing costs and increasing functionality. In recent years, much advancement has been made to integrate optical elements in the form of lenses,[1–3] lasers,[4,5] waveguides,[6,7] and sensors[8,9] with microfluidic devices. This research has coalesced into a field often referred to as optofluidics.

Because of their flexibility and biocompatibility, free space optical tweezers have proven to be a useful tool for deflecting, sorting and transporting microparticles within lab-on-chip devices.[10,11] Recently, researchers have demonstrated the ability to increase optical trapping forces on particles by using the evanescent field of planar waveguides.[12–17] To further augment the optical forces exerted on particles, other researchers have exploited devices like slotted waveguides[18] and plasmonic[19] structures to generate high-intensity field gradients for the trapping of nanoparticles and biomolecules with diameters as small as 50 nm. While this is highly advantageous for nanoscale trapping applications, they are limited for microparticle trapping and propulsion because the length scale that a nanophotonic trap can act over is much smaller. Another method by which the optical forces on microparticles can be increased is through the use of hollow-core[20,21] and liquid-core/liquid-cladding waveguides[22] which enable the particle to directly interact with the optical mode rather than just the evanescent field.

Alternatively, one can achieve high optical intensities in planar waveguiding devices by incorporating a resonant structure, such as a whispering gallery mode (WGM) resonator. These resonators siphon a portion of light from a waveguide and recirculate the optical energy repeatedly along a circular path.[23] Resonance occurs when incoming light is in phase with light in a resonator that has completed a revolution around the structure. At specific discrete wavelengths, light will constructively interfere, resulting in a stronger optical intensity confined in the resonant structure relative to the bus waveguide.[24] This strong coupling correlates with a sharp drop in the bus waveguide output. This behavior associated with resonant structures enables WGM resonators to be used as nanoscale chemical[25] or biochemical[26] sensors. The large field amplification also applies to the evanescent field of WGM devices. A recent paper by Arnold *et al.*[27] demonstrated the trapping and propulsion of 280 nm diameter nanoparticles on a spherical WGM resonator.

Here we demonstrate, for the first time, an integrated microring resonator switch for optically trapped microparticles. As seen in Fig. 1, our device consists of a microring resonator fabricated in SU-8 epoxy negative photoresist evanescently coupled to a bus waveguide of the same material. The path of trapped particles on the device is controlled by optical resonance and local field amplification in the ring creating an optical gradient force that pulls particles from the bus to the ring resonator. As we will demonstrate below, we can dynamically control the switch in real-time by changing the wavelength of the light at the input of the bus waveguide. To characterize the proposed mechanism for our switch, we determine the enhancement in propulsion velocity of particles trapped on the ring due to optical resonance. We also determine the overall efficiency of the ring resonator switch by measuring the fraction of particles routed onto the ring, which provides the optimal wavelengths for binary switch operation. Furthermore, we also describe our fabrication technique using controlled overexposure photolithography which enables ring structures with gap widths much smaller than the resolution of photolithography techniques, achieving controllable gap widths on the order of 100 nm in size.

[a]*245 Upson Hall, Cornell University, Ithaca, USA. E-mail: ay38@cornell.edu; Fax: +1 607 255 1222; Tel: +1 607 220 4586*
[b]*240 Upson Hall, Cornell University, Ithaca, USA. E-mail: de54@cornell.edu; Fax: +1 607 255 1222; Tel: +1 607 255 4861*

† Electronic supplementary information (ESI) available: Supplemental movie 1 shows the trapping and propulsion of 3 μm polystyrene beads on the optofluidic ring resonator switch. The movie shows the deflection of particles onto the ring while on-resonance followed by a change in wavelength which turns off the switch. Finally the switch is turned on again and particles are deflected onto the ring. See DOI: 10.1039/b920006a

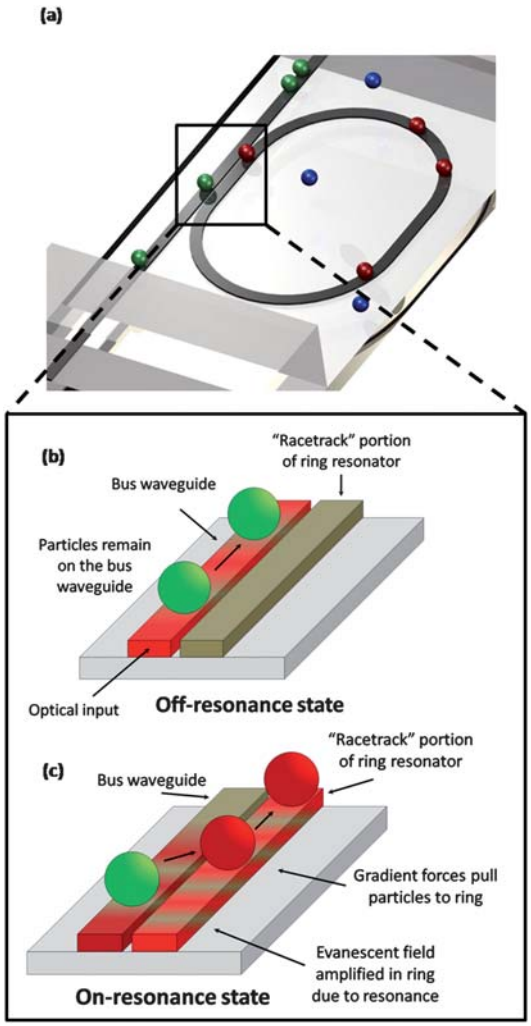

Fig. 1 Schematic of optofluidic ring resonator switch. (a) Rendered picture of device with PDMS microfluidics. (b and c) Illustration of switching mechanism due to optical gradient forces when the ring is strongly coupled at the resonant wavelength.

Results and discussion

Here, we describe the operating principle of the optofluidic ring resonator switch. As shown schematically in Fig. 1, a continuous wave laser amplified by an erbium-doped fiber amplifier (EDFA) is coupled into the bus waveguide. Some of the radiation extends into the ring waveguide in the region where the distance between bus and ring is smallest due to degenerate mode coupling. When the light that has traveled around the ring is in phase with incoming radiation, the waves constructively interfere resulting in a stronger optical field. The point at which light is most confined within the ring, known as the resonant wavelength, also results in a dramatic increase in the optical field confined within the ring. These resonating wavelengths of the structure are identified by a corresponding drop in the power output of the bus waveguide. The optical microring resonator switch operates by alternating between an on-resonance and off-resonance wavelength (about 1 nm). While the ring is on-resonance, particles trapped on the bus waveguide will be routed on the ring due to gradient forces arising from stronger local field intensities in the ring. In an off-resonance state, the bus waveguide will have a stronger relative intensity and the particles will tend to remain on the bus waveguide. To summarize, we exploit optical resonance in the ring and use wavelength of light to actively control the local optical field in our device and thus exert control over the path taken by optically trapped particles.

Particle switching using microring resonators

In Fig. 2, we show a series of images that illustrate the active trapping and switching of 3 μm polystyrene microparticles by changing the wavelength of coupled light. Using light from a tapered lens fiber, the waveguides are excited at a wavelength near 1550 nm with an input power of 300 mW. To achieve particle switching, the wavelength of light is tuned from λ_r = 1552.225 nm, the resonant wavelength which exhibits the strongest drop in power at the end of the bus waveguide, to non-resonant wavelength, λ_n = 1553.225 nm. At λ_r, the majority of particles is trapped on the bus waveguide initially and is diverted onto ring due to strong resonant coupling. After a series of particles have been diverted, the wavelength is changed 1 nm to λ_n, and the following set of particles to approach the switching junction bypass the ring and remain on the bus waveguide. We observe that particles that have been trapped on the ring while on-resonance will remain trapped and still be propelled when the ring is switched to an off-resonance state. Finally, after switching back to the resonant wavelength λ_r, the next series of trapped microparticles are diverted onto the ring structure.

Qualitatively, during our experiments we have observed the premature release of particles on the bus waveguide before being routed onto the ring or propelled beyond the switching point. Similarly, we have observed that when multiple closely spaced particles arrive at the junction point, the particles will drift back and forth, creating a wave-like motion in the chain of particles. This could arise if the optical gradient forces originating from both the bus waveguide and the resonator acting upon the particles simultaneously with the same relative magnitude of force and particles are not completely pulled over to the ring waveguide. A stronger optical resonance effect, represented by a higher quality factor (Q-factor), should lead to sharper differences in the optical intensity in the bus and ring waveguides at on-resonance wavelengths. Another potential explanation for this effect could be mode profile mismatch or bending losses due to the curvature of the ring resonator near the point where the wave-like motion of particles occurs. A future experiment to characterize this effect could examine particle switching between two evanescently coupled linear waveguides or a ring with an even larger radius of curvature than the one described here.

Device characterization

It is well known that the radiation pressure force scales proportionally to the optical intensity. Therefore, we can infer the strength of the optical field in the ring by measuring the steady-state radiation pressure velocity of the trapped particles as a function of wavelength. Also, we can determine the switching efficiency, defined as the fraction of particles routed onto the ring to the number of total trapped particles at any given wavelength, by using particle tracking software to determine the total number

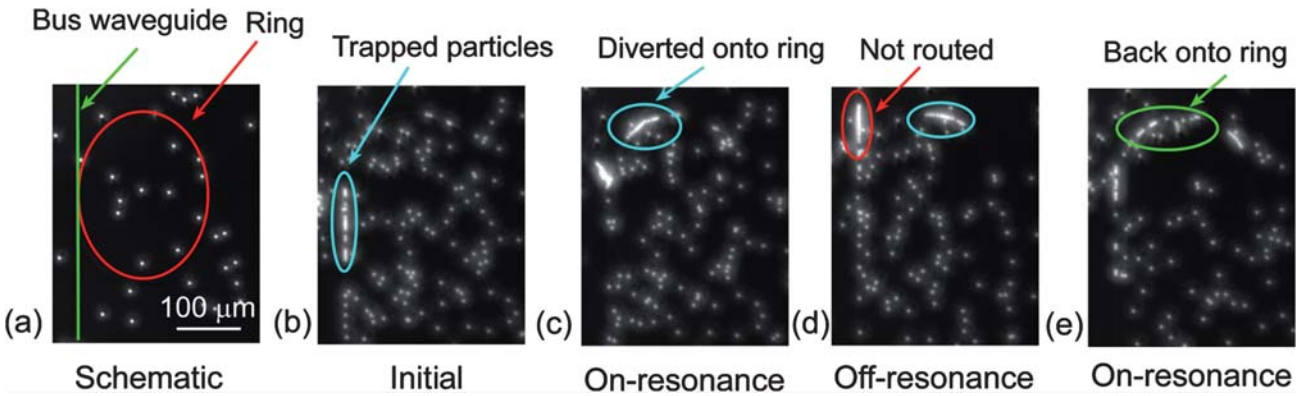

Fig. 2 Active optical switching of particles on a microring resonator. This image sequence taken from supplemental movie 1† illustrates the switching effect by moving through an on–off–on resonance sequence. Here λ_r represents the resonant wavelength and λ_n represents the non-resonant wavelength. (a) Schematic of ring and bus waveguide overlay with CCD camera image. The same crop is used for all subsequent images. The dots represent 3 μm fluorescent polystyrene spheres. (b) Initial state of the system with a 'string' of particles trapped on the bus waveguide. (c) The trapped particles are diverted and continue to move forward on the ring. At this point, the input wavelength is changed to λ_n. (d) The next series of trapped particles pass through the switching junction and remain on the bus waveguide. The input wavelength is changed to λ_n. (e) Sequential particles are switched onto the ring structure again.

of trapped particles and the number of particles routed onto the ring.

Our characterization of the particle transport and switching analyzes data obtained from two adjacent ring resonators with the same ring length on a single fabricated device. We define here ring A as the device that has a 296 nm gap width and ring B as the device with a 335 nm gap width. Both sets of results are used to illustrate how the degree of coupling enhances the velocity increase and switching of optically trapped particles. Fig. 3a shows the transmission spectra of the two adjacent ring resonator devices clad in water while excited by a 1550 nm tunable source. A 30 nm difference in the gap width of the two waveguides leads to a 10 dB difference in the power drop at the resonant wavelength. The quality factors of both rings, defined as $\lambda/\Delta\lambda$ at full width half maximum, are approximately 1550. The free spectral range of the devices is approximately 2 nm. As demonstrated previously by Levy *et al.*,[28] changing the refractive index of the cover medium by flowing different media through the microfluidic channel can tune the coupling between the ring and bus waveguides resulting in a higher *Q*-factor. A more advanced device structure could incorporate a method to tune resonant wavelength of a microring structure, either *via* the electro-optic effect or microfluidic tuning.[28]

Fig. 3b illustrates the increase in broadband noise in the EDFA amplified light due to amplified spontaneous emissions. The spectra of light coming out of the 1550 nm tunable laser w/wo EDFA amplification were obtained using an optical spectrum analyzer. These emissions lead to a 100-fold increase in noise emissions in the 1530–1580 nm range. The increased noise and low free spectral range of our devices ensure a non-zero amount of light is always coupled into the ring resonator. This is likely the reason why particles can remain trapped and experience radiation pressure when the input wavelength can be considered off-resonance. If a strong optical resonance is required, as in the case for sensing applications involving the detection of small changes in the resonant wavelength due to binding events, then a notch filter can be used to filter out the non-excitation wavelengths.

Fig. 4 shows the measured steady-state velocity of 3 μm polystyrene beads on the ring portion of the resonator device as a function of optical wavelength and detected power at the output of the waveguides for two adjacent resonator devices. The velocity enhancement for ring A was 200% and 250% for ring B defined here as the ratio of the average propulsion velocity of the particle during optical resonance *vs.* its non-resonant propulsion velocity. As a control, we can compare the velocity increase for particles trapped on the ring to the velocity of particles trapped on the bus waveguide before the ring as a function of wavelength. The difference between the highest and lowest velocities measured on the bus waveguide was 24% and 36% for ring A and ring B, respectively. As expected, the particles trapped on the bus waveguide do not experience the same velocity enhancement as particles trapped on the ring. The error bars in Fig. 4 represent mechanical vibrations in the coupling fiber and changes in fluid velocity in the experimental system. We do acknowledge that this does lead to repeatability issues between different chips because losses in waveguides and differences in coupling can result in the same value for output power at the end of a waveguide while differing in the amount of actual coupled optical power. However, the observed trend of a velocity increase at optical resonance is observable across different experimental devices, even if the actual values of propulsion velocity cannot be easily correlated. The amount of noise can be reduced by using lenses to obtain better mode matching in the case of end-fire coupling or by using a different coupling mechanism such as a grating coupler.[29]

The power drops measured for ring A and ring B at the resonant state are −3.5 dB and −5.4 dB, respectively. We note that the increase in velocity for ring A is less pronounced in ring B due to the difference in gap width and most likely ring A is more weakly coupled than ring B. The drops in transmission when the ring is coupled are less steep in Fig. 4 compared to Fig. 3 due to the EDFA noise as described above. We observe that as the optical wavelength approaches the resonant wavelength of the ring resonator, output power in the bus waveguide

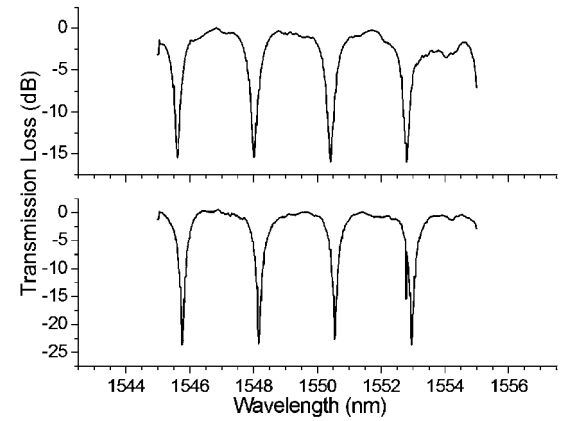

(a)

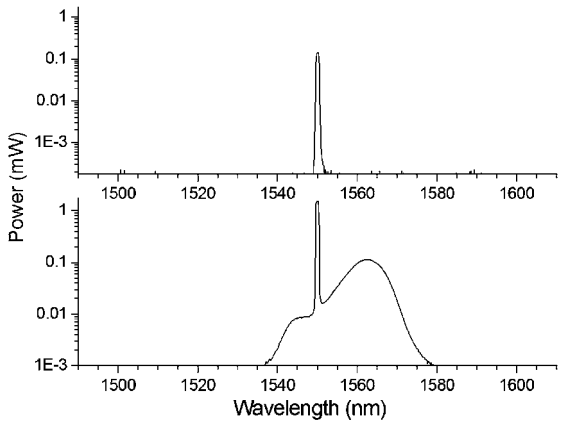

(b)

Fig. 3 Optical transmission spectra of ring resonators and laser output. (a) The top spectra (ring A) represent a bus/ring gap width 30 nm smaller than the bottom spectra (ring B). The rightmost resonance (~1552 nm) in both spectra is the one used in the EDFA amplified trapping and switching experiments. (b) The spectra of the unamplified light coming from a (top) 1550 tunable source and (bottom) after amplification using an EDFA. The output powers were plotted using a logarithmic scale.

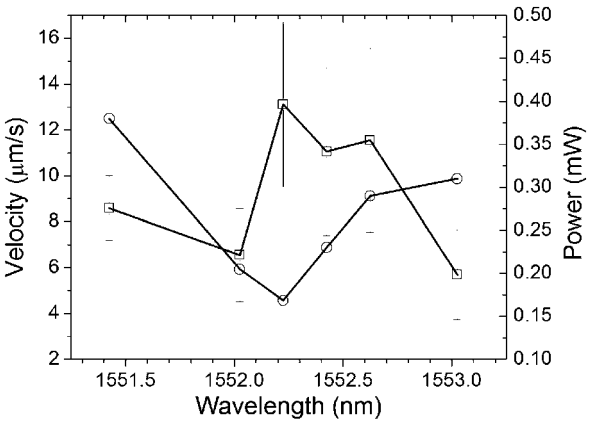

(a)

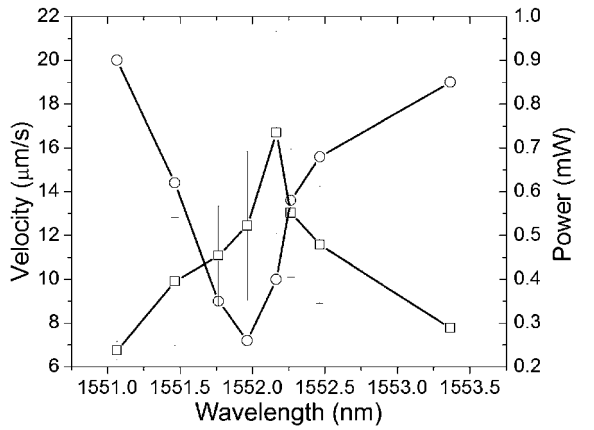

(b)

Fig. 4 Enhancement of propulsion velocity. Plot of steady-state velocity (squares) of 3 μm polystyrene beads trapped on rings and power output (circles) of the bus waveguide as a function of wavelength for (a) ring A and (b) ring B. Error bars for the velocity measurements are the standard deviation of velocity measurements due to fluctuation in guided power from mechanical vibration of the tapered lensed fiber used for coupling in the waveguide.

decreases as resonator coupling increases. This then leads to an increase in the propulsion velocity of trapped particles. Conversely, when the wavelength is off-resonance, the measured velocity is reduced from its on-resonance value. As stated previously, we determine the effectiveness of the resonator switch by directly measuring the fraction of particles routed onto the ring from the bus waveguide as a function of the input wavelength, as seen in Fig. 5. We define the switch fraction as the number of particles that were successfully routed onto the ring over the total number of particles trapped initially on the bus waveguide. Similarly, we define the rejection fraction as the number of particles that remained on the bus waveguide without being routed onto the ring. For ring B, we can achieve an 80% switching fraction at the resonant wavelength, and an 80% rejection fraction when the ring is excited at a non-resonant wavelength. The switching fraction is lower for ring A; about 60% of the particles are diverted when the ring is on-resonance, due to weaker ring coupling. We expect that since the power drop measured from ring A is lower than ring B that the amount of light coupled into the ring is smaller as well. This leads to a smaller net force experienced by the particle, and a smaller likelihood of pulling the particle over from the bus waveguide.

Materials and methods

The SU-8 ring resonator devices were fabricated using stepper photolithography. The ring design was based on the racetrack design used previously by Levy *et al.*[28] This design allows for a longer coupling distance compared to a completely circular ring structure. Our rings were 200 μm in diameter with a coupling length of 50 μm. The waveguide dimensions were designed to be 2 μm wide and 700 nm tall. The gap spacing between bus waveguide and resonator was specified to be 300–600 nm with a change in the gap distance of 30 nm between adjacent resonators. The ring gap after fabrication was often reduced by

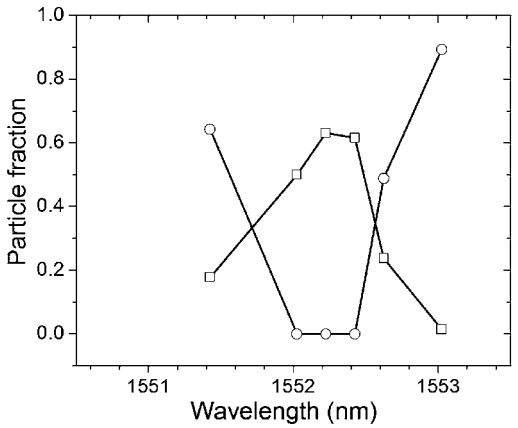

(a)

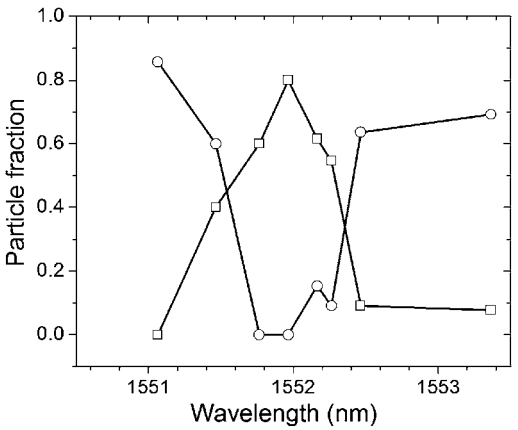

(b)

Fig. 5 Particle switch efficiency as a function of input wavelength. Fraction of particles that were routed onto the ring (squares) or bus waveguide (circles) plotted as a function of input wavelength for (a) ring A and (b) ring B. We define particle fraction as a general term to represent the switching fraction (squares) of routed particles and the rejection fraction (circles) of particles that remained on the bus waveguide. The fractions shown here are calculated including particles that released at the switching junction due to trapping instability. The output power detected at the end of the bus waveguide (not shown here) is the same as in Fig. 4.

200–300 nm due to controlled overexposure of the photoresist, creating much smaller gap features than normally possible using photolithography.

The photoresist was spun at 1000 rpm for 40 s on a fused silica substrate to achieve a film thickness of 700 nm. Exposure of the wafer was done using an i-line 5× stepper (GCA Autostep) at a computer controlled exposure time ranging from 0.20–0.3 s with an estimated intensity of 500 mW cm^{-2}. The variability in exposure times shows the range of overexposure required for a sub-resolution gap between the bus waveguide and ring structure. Further optimization of the exposure time used an SEM analysis of dies at exposure intervals of 0.01 s. The waveguide devices were then diced and cleaved using a partial backside cleaving technique leaving a final edge width of 75–100 μm. This technique partially dices the device near the waveguide input and output and uses mechanical force to create a clean coupling edge for polymer on glass waveguiding devices.

The PDMS microchannels were made using standard fabrication techniques, using a microchannel master created from SU-8 2025 on a silicon wafer. The resulting channels were 500 μm wide with a height of 25 μm and were bonded to the ring resonator chip, leaving the input and output regions of the chip clad in air.

The light source used for exciting the waveguides is a 1550 nm tunable erbium-doped fiber laser which is further amplified using an EDFA to achieve the necessary powers for trapping. Light is coupled into the waveguides using a tapered lens fiber. Polarization of the light entering the waveguides was determined using a polarization filter and controller. All the experiments conducted here were done using transverse electric (TE) polarized waves. This was done to maintain consistency across the experiment and minimize differences in coupling and propagating losses. The waveguides have a 3 mm offset with a 500 μm bending radius. The optical losses in these waveguides were previously characterized by Schmidt *et al.*[17]

In our experimental system, we use a pressure-driven flow induced by a syringe pump to flow 3 μm diameter fluorescent polystyrene beads in the microchannels over the ring resonator device. The particles were suspended in a pH 7.0 buffer solution with 1% w/v Triton X-100 surfactant to mitigate particle adsorption on surfaces. When the bus waveguide is optically excited, the particles are trapped both on the bus waveguide and on the ring resonator structures. Trapped particles exhibit radiation pressure propulsion in the direction of optical propagation. We use a CCD camera (Hamamatsu C472-80) and Video Spot Tracker software to determine the steady-state velocity of trapped particles. The switch efficiency was determined by analyzing the image stacks using the ImageJ software to determine the number of particles which were initially trapped on the bus waveguide that were diverted onto the ring structure.

Conclusions

In summary, we have demonstrated an optically driven microring resonator particle switch that is easily integrated with waveguide-based optofluidic transport architectures. The switch mechanism we present here uses the natural amplification of optical energy in the ring to divert trapped particles either onto the ring or along the bus depending on whether the excitation wavelength corresponds to a resonant or non-resonant condition. We show that we can achieve a 250% enhancement of the steady-state velocity of trapped particles along with an 80% switching fraction.

Acknowledgements

The authors would like to thank Arthur Nitkowski for technical discussions. This work was funded by the US National Science Foundation NIRT: Active Nanophotofluidic Systems for Single Molecule/Particle Analysis (Award number 0708599). This work was performed in part at the Cornell NanoScale Facility, a member of the National Nanotechnology Infrastructure Network, which is supported by the National Science Foundation (Grant ECS-0335765).

Notes and references

1 X. L. Mao, S. C. S. Lin, M. I. Lapsley, J. J. Shi, B. K. Juluri and T. J. Huang, *Lab Chip*, 2009, **9**, 2050–2058.
2 X. L. Mao, J. R. Waldeisen, B. K. Juluri and T. J. Huang, *Lab Chip*, 2007, **7**, 1303–1308.
3 S. K. Y. Tang, C. A. Stan and G. M. Whitesides, *Lab Chip*, 2008, **8**, 395–401.
4 Z. Y. Li, Z. Y. Zhang, T. Emery, A. Scherer and D. Psaltis, *Opt. Express*, 2006, **14**, 696–701.
5 D. Nilsson, S. Balslev, M. M. Gregersen and A. Kristensen, *Appl. Opt.*, 2005, **44**, 4965–4971.
6 E. J. Lunt, P. Measor, B. S. Phillips, S. Kuhn, H. Schmidt and A. R. Hawkins, *Opt. Express*, 2008, **16**, 20981–20986.
7 D. B. Wolfe, R. S. Conroy, P. Garstecki, B. T. Mayers, M. A. Fischbach, K. E. Paul, M. Prentiss and G. M. Whitesides, *Proc. Natl. Acad. Sci. U. S. A.*, 2004, **101**, 12434–12438.
8 C. Y. Chao and L. J. Guo, *Appl. Phys. Lett.*, 2003, **83**, 1527–1529.
9 L. N. Jiang and S. Pau, *Appl. Phys. Lett.*, 2007, **90**, 111108.
10 R. W. Applegate, J. Squier, T. Vestad, J. Oakey, D. W. M. Marr, P. Bado, M. A. Dugan and A. A. Said, *Lab Chip*, 2006, **6**, 422–426.
11 M. P. MacDonald, G. C. Spalding and K. Dholakia, *Nature*, 2003, **426**, 421–424.
12 S. Gaugiran, S. Getin, J. M. Fedeli and J. Derouard, *Opt. Express*, 2007, **15**, 8146–8156.
13 K. Grujic, O. G. Helleso, J. P. Hole and J. S. Wilkinson, *Opt. Express*, 2005, **13**, 1–7.
14 J. P. Hole, J. S. Wilkinson, K. Grujic and O. G. Helleso, *Opt. Express*, 2005, **13**, 3896–3901.
15 H. Y. Jaising and O. G. Helleso, *Opt. Commun.*, 2005, **246**, 373–383.
16 L. N. Ng, B. J. Luff, M. N. Zervas and J. S. Wilkinson, *Opt. Commun.*, 2002, **208**, 117–124.
17 B. S. Schmidt, A. H. Yang, D. Erickson and M. Lipson, *Opt. Express*, 2007, **15**, 14322–14334.
18 A. H. J. Yang, S. D. Moore, B. S. Schmidt, M. Klug, M. Lipson and D. Erickson, *Nature*, 2009, **457**, 71–75.
19 A. N. Grigorenko, N. W. Roberts, M. R. Dickinson and Y. Zhang, *Nat. Photonics*, 2008, **2**, 365–370.
20 P. Measor, S. Kuehn, E. J. Lunt, B. S. Phillips, A. R. Hawkins and H. Schmidt, *Opt. Lett.*, 2008, **33**, 672–674.
21 P. Measor, L. Seballos, D. L. Yin, J. Z. Zhang, E. J. Lunt, A. R. Hawkins and H. Schmidt, *Appl. Phys. Lett.*, 2007, **90**, 211107.
22 S. K. Y. Tang, B. T. Mayers, D. V. Vezenov and G. M. Whitesides, *Appl. Phys. Lett.*, 2006, **88**, 061112.
23 F. Vollmer and S. Arnold, *Nat. Methods*, 2008, **5**, 591–596.
24 C. R. Pollock and M. Lipson, *Integrated Photonics*, Kluwer Academic, Boston, London, 2003.
25 A. M. Armani and K. J. Vahala, *Opt. Lett.*, 2006, **31**, 1896–1898.
26 I. M. White, H. Oveys, X. Fan, T. L. Smith and J. Y. Zhang, *Appl. Phys. Lett.*, 2006, **89**, 191106.
27 S. Arnold, D. Keng, S. I. Shopova, S. Holler, W. Zurawsky and F. Vollmer, *Opt. Express*, 2009, **17**, 6230–6238.
28 U. Levy, K. Campbell, A. Groisman, S. Mookherjea and Y. Fainman, *Appl. Phys. Lett.*, 2006, **88**, 111107.
29 F. Van Laere, G. Roelkens, M. Ayre, J. Schrauwen, D. Taillaert, D. Van Thourhout, T. F. Krauss and R. Baets, *J. Lightwave Technol.*, 2007, **25**, 151–156.